Springer

KSME

Journal of Mechanical Science and Technology 29 (8) (2015) 3489~3499
www.springerlink.com/content/1738-494x(Print)/1976-3824(Online)
DOI 10.1007/s12206-015-0747-0

Nitric oxide emissions and combustion performance of nontraditional ring-fired boilers with furnace geometries †

Yonmo Sung[1], Cheolyong Choi[1], Cheoreon Moon[1], Seongyong Eom[1], Jong Jae Lee[2], Byung Doo Kim[2], Gyungmin Choi[1,*] and Duckjool Kim[1]

[1]*School of Mechanical Engineering, Pusan National University, Busan, 609-735, Korea*
[2]*Korea Coating Inc., 33-6, Sodong-ri, Eumbong-myeon, Asna-si, Chungcheongnam-do, 336-864, Korea*

(Manuscript Received April 3, 2014; Revised April 6, 2015; Accepted April 14, 2015)

Abstract

The flow, combustion and emission characteristics of nontraditional ring-fired-type furnaces were investigated numerically to evaluate the effects of incorporating additional inner water walls on the heat transfer, carbon burnout and emissions of nitrogen oxides. Both tangentially and ring-fired-type furnaces were considered and the ring-fired-type furnaces were divided into four inner-water-wall cases: without, normal type, radiant expended type and both radiant and convective expended type. The presence of the inner water wall led to an improvement of approximately 50% in the heat flux. In particular, the reduction in nitrogen oxide emissions was approximately 30%, whereas the carbon burnout was kept constant.

Keywords: Coal combustion simulation; NO_x emission; Particle residence time; Ring fired boiler

1. Introduction

In pulverized coal thermal power plants, the use of coal types beyond the scope of the design is inevitable, because the imbalance between coal demand and supply has become serious as a result of the increasing energy consumption by large countries such as China and India [1]. One issue of interest is the emission of nitrogen oxides (NO_x), which are generated primarily from transportation, utilities, and other industrial sources. NO_x emissions have decisive effects on a variety of environmental problems such as acid rain, smog, and visibility degradation. Thus, they are regulated by different levels of government throughout the country. There are roughly two ways to reduce and control NO_x emissions in the coal combustion fields. First, NO_x control has been achieved over the past several decades by pre-combustion controls with oxy-fuel combustion or low nitrogen containing fuels, post-combustion by Selective catalytic reduction (SCR) and Selective noncatalytic reduction (SNCR), and in-furnace combustion controls for staged combustion and reburning technologies [2-11]. Second, various boiler types, including wall-fired, tangentially fired, vertically fired, and cell burner units, have been considered as NO_x control technologies for coal-fired electric utility plants [12-18]. The burners of the wall-fired-type boiler produce strong turbulent flames, which result in high levels of NO_x formation. In contrast, tangentially fired boilers consist of vertical wind boxes that include an array of coal nozzles and air ports mounted in each corner of the furnace. In this furnace, a lower temperature and diminished turbulence lead to an inherently lower NO_x formation than that of a wall-fired furnace. The NO_x formation depends primarily on the temperature, reaction time, and turbulence. In other words, the flame temperature and residence time of the fuel/air mixture, along with the nitrogen content of the coal and the quantity of excess air used for combustion, determine the NO_x levels in the flue gas. Combustion modifications may delay the mixing of fuel and air, thereby reducing the temperature and initial turbulence, which minimizes the NO_x formation [19].

There are previous studies on combustion modifications and furnace geometry optimization. Choi and Kim numerically investigated the effect of air staging for Over fired air (OFA) operation, focusing on the reduction of NO_x emissions in a tangentially fired furnace [12]. Liu et al. investigated the combustion and NO_x formation characteristics using validated models under various OFA ratio and OFA port position combinations in a wall-fired furnace [13]. Liu et al. also investigated the influence of OFA on the combustion in a dual-circle tangentially fired single furnace [14]. Yan et al. numerically studied the effects of the geometric configurations of tangentially fired boilers with three different burner arrangements [15]. Modlinski numerically investigated two tangentially

*Corresponding author. Tel.: +82 51 510 2476, Fax.: +82 51 512 5236
E-mail address: choigm@pusan.ac.kr
† Recommended by Associate Editor Jeong Park

fired furnaces with similar designs and thermal power ratings to reduce slagging. The boiler was retrofitted by replacing swirl burners [16]. All of the above studies found ways to mitigate NO_x emissions and enhance the combustion characteristics.

However, there has been relatively insufficient research on the development of new concepts for nontraditional boilers in terms of reducing pollutant emissions and enhancing other combustion performance characteristics. Few studies have investigated the development of ring-fired or circular furnace boilers [20-23]. The use of a ring (Actually an octagonal) furnace offers the following advantages, relative to a conventional design: reduced fouling and slagging through the reduction of temperatures inside the furnace, dramatically reduced NO_x emissions through more effective mixing and internal recirculation, a 30% to 40% reduction in boiler height, a 15% reduction in the cost of heating surfaces, improved operating reliability for the furnace water wall panels due to more uniform metal temperatures around the furnace perimeter, and a simplified design for the boiler building as well as the support and pendant structures [20]. The distinctive feature of ring furnaces, which should be regarded as a further development compared with traditional tangential furnaces, is the vortex flow of the furnace gases in the annular space between the outer and inner shields [21]. Efficient low-temperature combustion of the fuel in a ring furnace is attained as a result of installing the additional surface of the shielded interior insert, together with the great intensification of mixing and the use of in-furnace gas recirculation [21].

This study, in conjunction with the above developments, was motivated by an invention that was made to avoid or minimize thermal NO_x emissions [23]. Unlike typical utility boilers, the boiler has both an outer water wall and an additional inner water wall. Therefore, the boiler can prevent high flame temperatures and the production of thermal NO_x. Moreover, the boiler provides more heat transfer to the water walls because of their larger contact surfaces, which can lead to a small boiler with higher efficiency. The flames in the furnace are surrounded by the outer water walls and are reflected by the inner water walls to heat the water in the outer water walls. However, the boilers require different combustion environments under certain firing conditions using low-rank fuels such as lignite, biomass, and the blends. The slagging and fouling related problems would be more severe than that of a design fuel because the ash fusion temperature is typically lowered. The longer residence time of coal particles in the boiler would be effective to mitigate those problems.

In this study, therefore, the coal particle behavior such as particle residence time and particle trajectory in the boiler was investigated in detail by considering several inner/outer wall expended models (Cases 3-5). Both tangentially and ring-fired-type furnaces were considered. The ring-fired-type furnaces were divided into four cases in relation to the inner water walls: without, normal type, radiant expended type, and both radiant and convective expended type. The effects of a fur-nace's geometric structure on the flow, combustion, and NO_x emission characteristics were investigated numerically using a commercial finite volume, three-dimensional (3-D) Computa-tional fluid dynamics (CFD) code. Our purpose was to evalu-ate the effects of incorporating additional inner water walls on the coal particle behavior, heat transfer, carbon burnout, and gas emissions. Additionally, information pertaining to the embodiment and preliminary evaluation of the advanced con-cept boiler for a pulverized coal thermal power plant was pro-vided based on the combustion and emission characteristics in comparison to a conventional tangentially fired boiler.

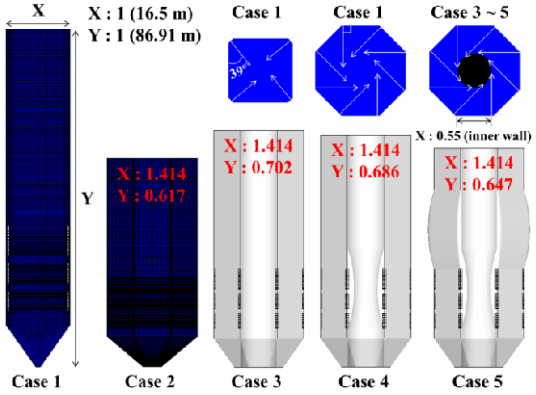

Fig. 1. Schematic of furnaces with different geometries.

2. Numerical methods and conditions

2.1 Boiler configurations and operating conditions

The geometric configurations of the tangentially and ring-fired furnaces simulated in this study are shown in Fig. 1. Cases 1 and 2 represent the traditional tangentially fired furnace and nontraditional ring-fired furnace, respectively. The normal type for case 3, radiant expended type for case 4, and both radiant and convective expended type for case 5 have inner water walls. Even though the geometry ratio (Length and width) was also changed according to the variation of cases 1-5, the effect of incorporating additional inner water walls on combustion and emission characteristics were investigated by keeping the entire control volume for all cases. Therefore, the furnace geometry was changed based on the tangentially fired boiler (Case 1) during constant combustion environments such as the coal and oxidizer input, coal type, and the burner arrangement. Coal particle injectors were installed at each corner in every case. The geometric parameters of the burner for all cases are shown in Fig. 2. A burner set contains several burners located in a vertical plane, with six step elevations. The order of the burner columns is A, B, C, D, E, and F, starting from the bottom; AB and CD have the same configuration and size. The primary air transports coal particles to the furnace with different air to fuel ratios in concentrated (fuel rich burner, Conc.) and weak sections (Fuel lean burner, Weak). The secondary air for combustion is injected into the furnace through the auxiliary, bottom, and OFA.

Table 1. Operating conditions in all cases.

Level		Coal [kg/s], weak (Concentrated)	Primary air [kg/s], weak (Concentrated)	Secondary air [kg/s]
Burner	A	2.4 (8.8)	6.07 (21.27)	112.4
	B	2.4 (8.8)	6.07 (21.27)	
	C	2.4 (8.8)	6.07 (21.27)	113.9
	D	2.4 (8.8)	6.07 (21.27)	
	E	1.2 (4.4)	4.01 (14.04)	85.27
	F	1.2 (4.4)	4.01 (14.04)	
OFA		-	-	190.1
Total		56 (200 ton/h)	145.5	501.6

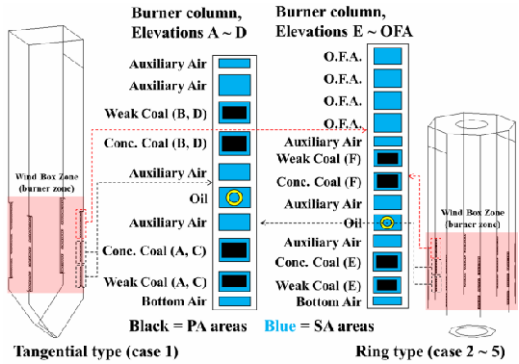

Fig. 2. Arrangement of burner columns.

The amount of fuel and oxidizer injected from each column corresponds to 500 MW_e. This amount is standard for a pulverized coal fired boiler used in a power plant in Korea (Table 1). The wall con-dition of the boiler was set to a fixed temperature (T_{wall} = 524 K), with no heat flux ($q'' = 0$) and an emissivity of 0.6 (ε) [12, 24]. The temperatures for the primary air, and the secondary air and OFA, were set to 333 K and 582 K, respectively. The exhaust gas was discharged at atmospheric pressure.

2.2 Computational domain grid system

A three-dimensional grid was created using FLUENT/GAMBIT (ANSYS, Inc., USA). The mesh systems of the burner region were more refined because of the high gradients of the velocity, temperature, and species concentrations. The grids for cases A, B, C, D, and E incorporated approximately 1500000, 1600000, 2100000, 1950000 and 1900000, respectively. The mesh consists of hexahedral cells and small portions of tetrahedral cells around the corners of the boiler. The number of cells in this simulation was similar to or larger than those used in most of the CFD studies for pulverized coal fired furnaces reported in Refs. [9, 12, 25].

2.3 Numerical models

Numerical simulations were carried out using a commercial CFD code, Fluent version 6.3. Proper sub-models were chosen to simulate the devolatilization, volatile combustion, char oxidation, thermal radiation, and NOx emission processes in the furnace. For the incompressible, steady two-phase turbulent flow and combustion in the furnace, the 3-D Reynolds-averaged Navier-Stokes governing equations for mass, momentum, species concentration, and energy were solved using the Semi-implicit method for pressure-linked equations (SIMPLE) algorithm [26] to handle the velocity-pressure coupling. The continuity, momentum, and energy equations are expressed as follows in Eqs. (1)-(3), respectively.

$$\frac{\partial u_i}{\partial x_i} = 0, \tag{1}$$

$$\frac{\partial u_i}{\partial t} + \frac{\partial u_i u_j}{\partial x_j} = -\frac{\partial p}{\rho \partial x_i} + \frac{\partial}{\partial x_j}\left((\nu + \nu_t)\left(\frac{\partial u_j}{\partial x_i} + \frac{\partial u_i}{\partial x_j} \right) \right), \tag{2}$$

$$\frac{\partial T}{\partial t} + \frac{\partial u_i T}{\partial x_i} = \frac{\partial}{\partial x_i}\left(\left(\frac{\mu}{\mathrm{Pr}} + \frac{\mu_t}{\mathrm{Pr}_t} \right) + \frac{\partial T}{\partial x_i} \right). \tag{3}$$

The standard κ-ε model was adopted in this simulation because it proved to be the most suitable model in terms of the computational cost, stability, and reliability of results in pulverized coal combustion applications [13, 25-29]. The turbulent kinetic energy k and the rate of energy dissipation ε are computed from a standard two-layer k-ε turbulent model.

$$\frac{\partial k}{\partial t} + \frac{\partial u_i k}{\partial x_i} = \frac{\partial}{\partial x_i}\left(\left(\nu + \frac{\nu_t}{\sigma_t} \right) \frac{\partial k}{\partial x_i} \right) + G - \varepsilon, \tag{4}$$

$$\frac{\partial \varepsilon}{\partial t} + \frac{\partial u_i \varepsilon}{\partial x_i} = \frac{\partial}{\partial x_i}\left(\left(\nu + \frac{\nu_t}{\sigma_\varepsilon} \right) \frac{\partial \varepsilon}{\partial x_i} \right) + \frac{\varepsilon}{k}\left(C_{\varepsilon 1} G - C_{\varepsilon 2} \varepsilon \right). \tag{5}$$

G denotes the production rate of k and is given below:

$$G = -\overline{u_i u_j} \frac{\partial u_i}{\partial x_j} = \nu_t \left(\frac{\partial u_i}{\partial x_j} + \frac{\partial u_j}{\partial x_i} \right) \frac{\partial u_i}{\partial x_j} \quad \text{and} \quad \nu_t = C_\mu \frac{k^2}{\varepsilon}. \tag{6}$$

In the above equations, the coefficients are as follows:

$$C_{\varepsilon 1} = 1.44,\ C_{\varepsilon 2} = 1.92,\ C_\mu = 0.09,\ \sigma_k = 1.0, \text{ and } \sigma_\varepsilon = 1.23.$$

A converged solution was obtained for the cold flow with species transport after 10000 iterations. Then, coal particle injection, gas phase reactions, and radiative heat transfer sub-models were added to the system of equations. Converged solutions for the reacting flow were obtained after approximately 30000 iterations (Requiring approximately 80 h using parallel computing with seven cores) from a constant outlet temperature for all cases. The finite-rate/eddy-dissipation model was used for the gas-phase combustion of the volatile matter released from the coal [30, 31]. Coal particle trajectories were calculated using the Lagrangian passion. For the coal

Table 2. Proximate and ultimate analysis, and other constants of Göttelborn coal.

Proximate analysis [weight %, dry]	
Volatile matter	36.7
Fixed carbon	55
Ash	8.3
Ultimate analysis [weight%, dry]	
Carbon	76.2
Hydrogen	4.7
Nitrogen	1.2
Sulfur	1
Oxygen	8
Ash	8.9
Calorific value [MJ/kg, dry ash free]	32.32
Coal particle density [kg/m^3, dry]	1000
Coal particle specific heat [J/kg·K, dry]	1100
Coal particle size distribution (Rosin-Rammler)	
Mean size [μm]	75
Minimum size [μm]	10
Maximum size [μm]	150
Spread parameter	4.52

particle injection, individual coal particles were injected by using a surface injection method and into the furnace from each Primary air (PA) as shown in Fig. 2. The interaction between the gases and the coal particles was considered every 20 iterations for the flow.

For radiative heat transfer (RHT) models, the Discrete ordinate (DO) model was proven to better fit the measurements obtained from the experimental validation and accuracy analysis studies for both the P-1 and DO models [32-34]. However, the DO model needs more computational resources and is more expensive than the P-1 model. In this study, therefore, the P-1 radiation model was used to calculate the RHT between gases and particles in the boiler because it is a cost effective and robust model for any complex geometry although it has some limitations regarding the optical thickness. The P-1 model has been extensively used to numerically simulate coal combustion for the RHT characteristics [13, 35-38]. The domain-based weighted sum of gray gases model was used to calculate the absorption coefficients of the gas phase. To minimize the computational time and stable convergence strategy, default values used for the devolatilization (Constant model) [39] and char combustion (Diffusion-limited model) [39] were the basic data given in the user's guide for the FLUENT software [31]. Table 2 lists all the necessary coal properties [31, 40].

The NOx calculation was carried out as a post-processing task based on the converged solution of the velocity, temperature, and species because the NOx calculation was assumed to have no significant influence on the flow field and major combustion process [13, 25, 41-43]. Moreover, NOx concentrations generated in combustion systems are generally low, and nitrogen chemistry reactions are superimposed onto the basic combustion model [44]. Three mechanisms are responsible for the NOx formation in combustion systems: thermal NOx, prompt NOx, and fuel NOx. Thermal NOx is generated by the oxidation of nitrogen in the combustion air. This formation can be modeled by the extended Zeldovich mechanism, which is well known. The reactions are as follows:

$$O + N_2 \underset{k_{r,1}}{\overset{k_{f,1}}{\rightleftharpoons}} N + NO, \tag{7}$$

$$N + O_2 \underset{k_{r,2}}{\overset{k_{f,2}}{\rightleftharpoons}} O + NO, \tag{8}$$

$$N + OH \underset{k_{r,3}}{\overset{k_{f,3}}{\rightleftharpoons}} H + NO, \tag{9}$$

where k_f and k_r represent the forward and reverse reaction rates, respectively. Then, the net rate of the thermal NO species via Eqs. (7)-(9) is given by

$$\frac{d[NO]}{dt} = k_{f,1}[O][N_2] + k_{f,2}[N][O_2] + k_{f,3}[N][OH] - k_{r,1}[NO][N] - k_{r,2}[NO][O] - k_{r,3}[NO][H]. \tag{10}$$

The O, H, and OH concentrations are calculated by using the partial equilibrium approach [12, 31]. Generally, the contribution of prompt NOx is negligible because of its small amount in coal combustion systems. Fuel NOx makes the main contribution to NOx formation in the coal combustion fields. It is produced by the oxidation of the nitrogen bound in the coal and typically accounts for more than 80% of the NOx formed in these systems [13, 41]. Fuel-bound nitrogen is usually split into volatile nitrogen and char nitrogen during coal devolatilization [13]. HCN and NH3, which are the dominant intermediate species formed from the volatile nitrogen, are competitively oxidized and reduced by means of the following generic scheme involving four reactions [25]:

$$HCN + O_2 \xrightarrow{k_4} NO + \cdots \tag{11}$$

$$HCN + NO \xrightarrow{k_5} N_2 + \cdots \tag{12}$$

$$NH_3 + O_2 \xrightarrow{k_6} NO + \cdots \tag{13}$$

$$NH_3 + NO \xrightarrow{k_7} N_2 + \cdots \tag{14}$$

where the reaction rate constants ki were proposed by DeSoete [41]. Additionally, with the interaction between the char and gas phase intermediates, NO can be reduced to N_2 through both heterogeneous and homogeneous reactions. However, in low NOx burners, which are designed to create a fuel-rich region, the homogeneous reactions seem to be the dominant reduction reactions [41].

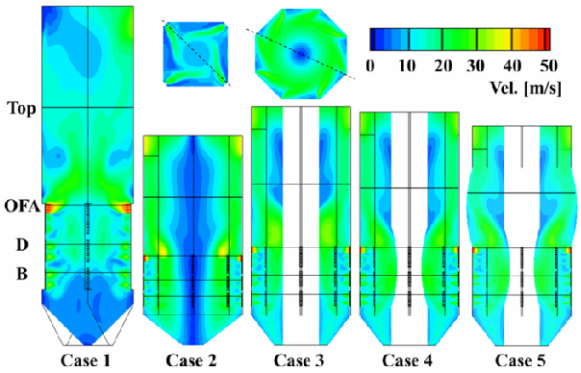

(a)

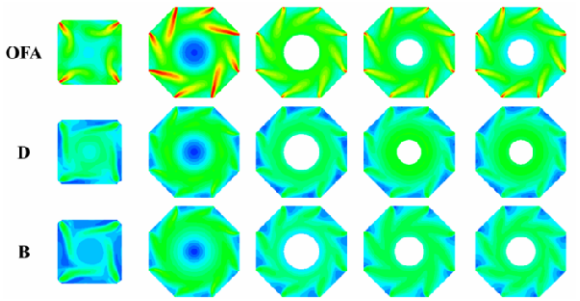

(b)

Fig. 3. Velocity contours under different furnace geometries: (a) central vertical cross-sections; (b) horizontal cross-sections at different burner levels.

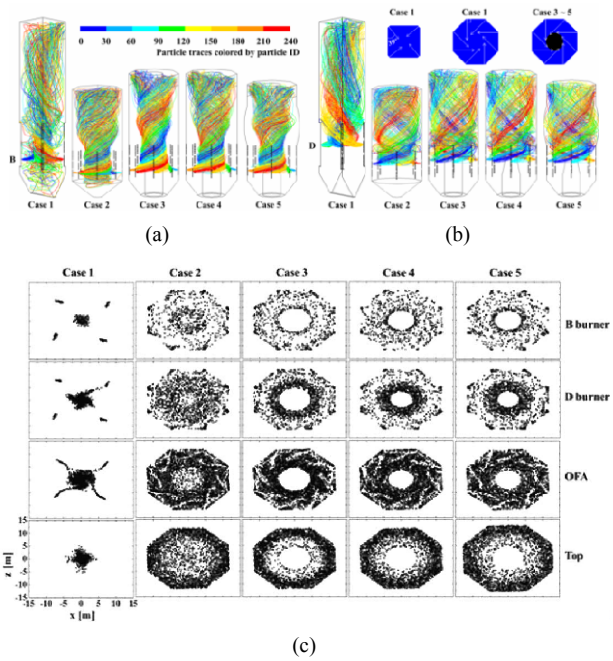

(a) (b)

(c)

Fig. 4. Trajectory and distribution of coal particles under different furnace geometries: (a) coal particle trajectories from B burner injection; (b) coal particle trajectories from D burner injection; (c) coal particle distributions at different planes.

3. Results and discussion

3.1 Flow fields and coal particle trajectories

The flow field in the furnace has a significant influence on the overall performance, including the flame temperature, emission, and burnout characteristics. Fig. 3 shows the velocity distributions in furnaces of the tangentially fired type for case 1, ring-fired type for case 2, and ring-fired type with an inner wall for cases 3-5 at different cross sections. The velocity contours at the centers of the vertical sections of the five furnace geometries are shown in Fig. 3(a). In all cases, dynamic flows near the burners, including OFA, are shown than in other regions, and counter-clockwise swirl flows are formed. The horizontal cross sections at the heights of the B and D burners and OFA are shown in Fig. 3(b). A swirling flow is clearly formed in the furnace, and the tangential circle region is enlarged with an increase in height. These results show a tendency similar to those in previous reports [7, 12, 15, 16]. In particular, the dead zones at the four corners for a tangentially fired furnace (Case 1) are effectively reduced by using ring-fired furnaces with eight corners (Cases 2-5). This implies that the ring-fired furnace is highly effective at utilizing the entire space in the furnace and improving the mixing performance of the coal particles with the oxidizer owing to the improved aerodynamics provided by increasing the number of burners. A higher flow velocity distribution is shown in case 2 compared with other cases. The area of the wind box zone is changed with the boiler height and width for cases 1-5. However, the control volume is constant for all the cases, as mentioned above in the section on numerical methods and conditions. Therefore, it is expected that case 2 may have a shorter particle residence time than the other configurations because of the shorter height of the boiler and the high velocity.

The trajectories of coal particles injected from different burner levels are depicted in Figs. 4(a) and 4(b). The coal particle trajectories show quite similar 3-D flows for all cases. They show the swirl flow motion around all the burner ports, which consist of four ports for case 1 and eight ports for cases 2-5, at the same burner level. The flow pattern affects not only the carbon burnout efficiency in terms of the particle residence time, but also the distribution of particles for enhancing the mixing of the oxidizer and coal particles. Fig. 4(c) shows coal particle distributions with different furnace geometries. This distribution was calculated at different planes as shown in Fig. 3. In a comparison of no inner water wall cases (Cases 1 and 2) in Fig. 4(c), coal particles are concentrated in the center region for case 1, and then the configuration of the tangential flow (So-called fireball) increases with the burner level. However, coal particles for case 2 are more dispersed to the outer wall of the furnace with increasing the higher coal injection from B burner to Top. The configuration of the tangential flow, or so-called fireball, increases with the burner level. In the inner-wall cases 3-5 from Figs 4(a) and 4(b), the trajectories of the coal particles change slightly with changes in the boiler geometry. Moreover, the particle number density is higher at the vicinity of the walls in Fig 4(c).

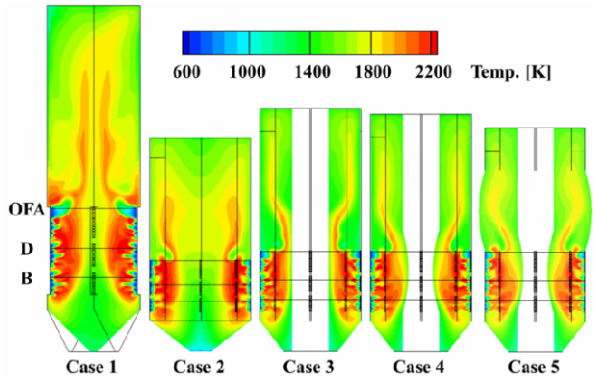

(a)

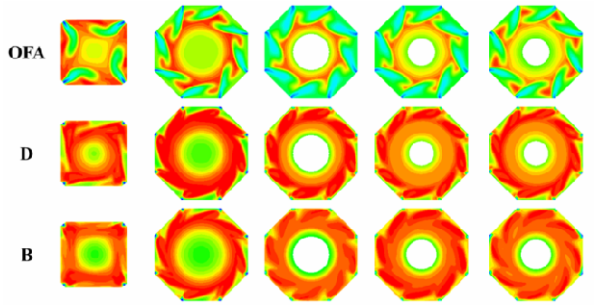

(b)

Fig. 5. Contours of gas temperature under different furnace geometries: (a) central vertical cross-sections; (b) horizontal cross-sections at different burner levels.

3.2 Temperature and heat flux distributions

Fig. 5 shows the temperature distributions in the vertical cross section and three horizontal cross sections along the boiler height for cases 1-5. Symmetrical temperature distributions are formed, and the maximum temperature and temperature gradient can be seen near the burner exit. The temperature increases along the furnace height in the burner zone, and then decreases dramatically at the OFA zone because a large amount of staging air is injected into the boiler. In this study, the maximum temperature of 2259 K for case 1 was relatively higher, and the average temperature of the burner planes was more than 100 K higher than those in previous reports [12, 15]. These results can be ascribed to differences in the coal devolatilization and char combustion models, and the radiative heat transfer model. Nevertheless, these results clearly show the effects of the boiler geometry on the temperature distributions in the boiler, which had a constant control volume, constant coal and oxidizer inputs, and the same wind box system in all cases. The temperature distributions are well identified for the B burner plane, as shown in Fig. 5(b). The temperature of case 2 is relatively higher than that of case 1 because of its higher input velocity at the wind box zone, as shown in Fig. 3. This means that the local NO_x formation is more active, and it is necessary to reduce the temperature of the burner zone in case 2. To reduce NO_x emissions, models of the inner water wall case were tested in this study. Cases 3-5 show lower temperature distributions than cases 1 and 2, and uniform temperature distributions at each burner plane were obtained. Cases 3-5, which had inner water walls, were more promising because of the temperature distributions produced by the stabilized flames from the neighboring burner arrangement, and the lower risk of local high temperatures producing NO_x emissions, slagging and corrosion.

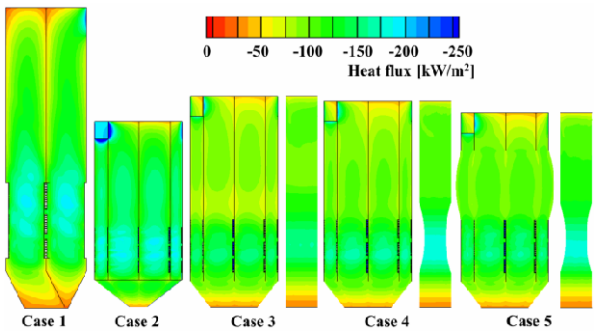

Fig. 6. Contours of radiation heat flux under different furnace geometries.

In this study, the injection rates for the coal particles were kept constant for all cases, as listed in Table 1. Thus, the same thermal energy inputs were supplied to the furnaces. The Wall heat flux (WHF) distributions are shown in Fig. 6, where a negative value indicates a WHF toward the walls. The WHF values in the burner regions are higher than those of the other regions because of high temperature, as shown in Fig. 5(a), and similar tendencies were seen for all cases. Therefore, the WHF for case 2 is higher than that of case 1. Cases 1 and 2 have area-weighted WHF values, which are based on the total area of the furnace, of 115 and 137 kW/m^2, respectively. In the inner-water-wall cases, the WHF of the outer water wall is lower than that of cases without an inner water wall. The total WHF on the outer and inner water walls is greatly increased by incorporating inner water walls. These are helpful for reducing the average temperature at the burner zones and enhancing the heat transfer characteristics of the additional heat exchange area. Thus, the boiler thermal efficiency increases with an increase in the total WHF; in particular, it can mitigate thermal NO_x emissions. Additionally, the total WHF is increased by a change in the configuration of the wall geometry for cases 3-5. The greater the WHF, the more the heat exchanges. The water-cooled wall absorbs a large amount of heat with increasing the WHF. However, the operational limitations imposed by the materials should be considered. In particular, the design values for the maximum heat flux per surface unit should not be exceeded.

3.3 Species distributions and phenomena at the boiler outlets

The distributions of the O_2, CO_2, and NO (NO and NO_2, collectively referred to as NO_x) mass fractions at the centers of the vertical sections for cases 1-5 are shown in Figs. 7-9, respectively. O_2 and CO_2 are complementary species as the

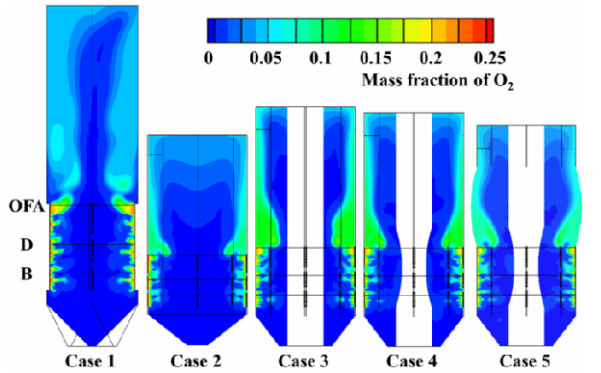

(a)

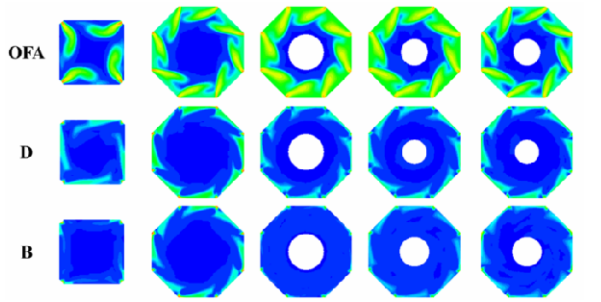

(b)

Fig. 7. Contours of mass fraction of O_2 under different furnace geometries: (a) central vertical cross-sections; (b) horizontal crosssections at different burner levels.

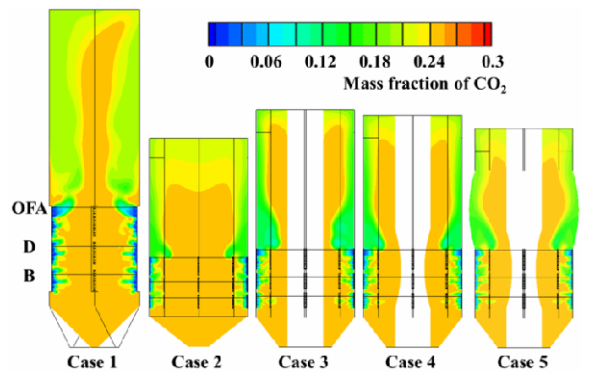

(a)

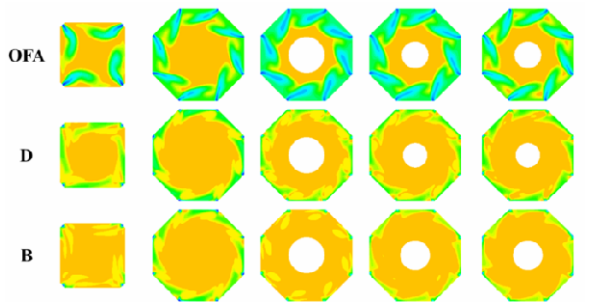

(b)

Fig. 8. Contours of mass fraction of CO_2 under different furnace geometries: (a) central vertical cross-sections; (b) horizontal crosssections at different burner levels.

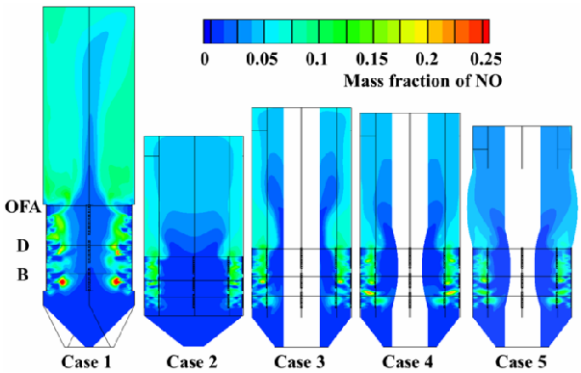

(a)

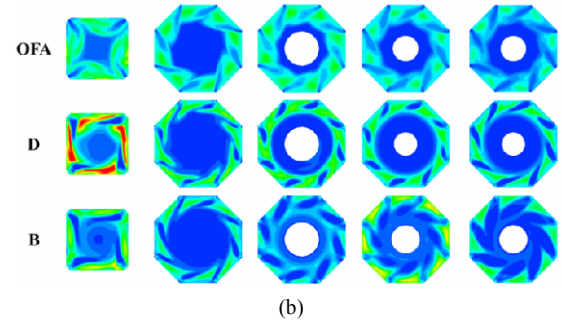

(b)

Fig. 9. Contours of mass fraction of NO under different furnace geometries: (a) central vertical cross-sections; (b) horizontal crosssections at different burner levels.

main reactant and product of the combustion. The O_2 concentration is relatively higher near the burners, where devolatilization and combustion are more active and volatile matter is more rapidly consumed. In a comparison of the temperature fields (Fig. 5) with the O_2 mass fraction (Fig. 7), the high temperature regions in the boiler roughly correspond to the regions with a lower O_2 mass fraction. In contrast to the O_2 mass fraction, the CO_2 mass fraction significantly increases with the envelope of flame in Fig. 8. These results show similar tendencies in all cases, as already reported for case 1 in previous studies [12, 13, 15]. Fig. 10 shows the mean concentrations of the main species at the outlet under different boiler geometries. The volatile, CO and N_2 emissions show almost the same levels at the furnace exit regardless of the furnace geometry. In particular, it is remarkable that the O_2 concentrations at the boiler exit were approximately 3.5% for cases 2-5 and below 3.1% for case A. The CO_2 and H_2O distributions were approximately the reverse of the O_2 distribution with a change in the boiler geometry in terms of additional water wall surfaces. As the temperature of the furnace increased, the CO_2 and H_2O generally increased. The statistical parameters at the boiler outlet are listed in Table 3.

The distributions of the NO mass fraction on the vertical and horizontal cross sections are presented in Fig. 9. The NO is mainly concentrated in the zone where the combustion is quite intense and the temperature is relatively high (see Figs. 5 and 9). Because the fuel and thermal NO_x formations depend

Table 3. Summary of outlet values of boiler for species concentration, NO_x and temperature under different boiler geometries.

	Case A	Case B	Case C	Case D	Case E
Volatile [ppm]	47	3	77	13	5
CO [ppm]	175	28	351	100	44
O_2 [%]	3.16	3.39	3.48	3.51	3.34
H_2O [%]	5.56	5.58	5.51	5.55	5.55
CO_2 [%]	14.83	14.59	14.51	14.49	14.56
N_2 [%]	76.43	76.44	76.45	76.45	76.48
NO_x [ppm]	1110	851	852	715	576
Temperature [K]	1594	1611	1543	1523	1534

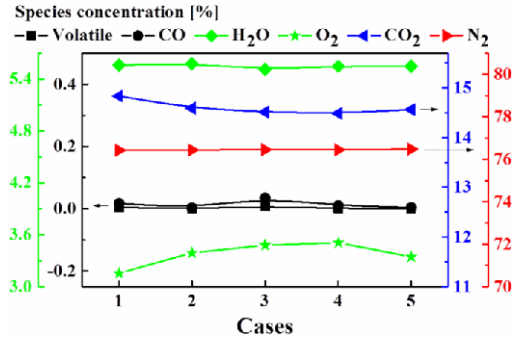

Fig. 10. Variations in main species concentrations under different furnace geometries.

on the temperature and air ratio in the combustion zone, the majority of NO_x is formed in the flame reacting region [12]. Near the burner region, the rapid release of the volatiles contained in the coal, along with the incoming O_2 injected from the burners, leads to the rapid formation of HCN, or NH_3 is converted to NO in fuel-lean regions and to N_2 in fuel-rich regions [12]. The change in the furnace geometry from the tangentially fired type (Case 1) to ring-fired types (Case 2-5) provides a larger space for the reducing environment (Fuel-rich region) of the fuel NO_x because it is more likely to increase the particle residence time in the burner zones, as shown in Fig. 4. Increasing the particle residence time in the burner zones is favorable for the decomposition of gaseous N species such as NO, NH_3, and HCN. Thus, the NO is greatly reduced when the geometry of the furnace model changes from case 1 to cases 2-5 under the constant control volume. The models (Cases 3-5) incorporating an inner wall show remarkable reduction results for the NO concentrations from the effects of both the reducing environment for the fuel NO_x and the change in thermal NO_x due to lower furnace temperatures.

3.4 Relationship between overall performances and coal particle behaviors

Fig. 11 shows the variations in the overall performances such as the carbon burnout, mean Wall heat flux (WHF), mean temperature, and mean NO_x concentration in the furnace under five different cases. Mean data were calculated by area-

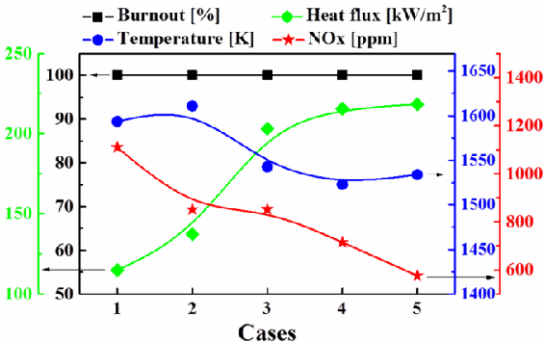

Fig. 11. Variations in overall performances under different furnace geometries.

weighted values. A furnace wall boundary for the WHF and furnace outlet boundary for both temperature and NO_x were considered. In general, the devolatilization of coal particles is completed in the furnace as a result of the high temperatures and kinetic rates of volatile release. Thus, the key reason for the differences in the combustion efficiencies is the carbon burnout, which was calculated based on the ash tracer method [45]. The burnout performance is 100% for all cases. It can be seen that changing the tangentially fired type to a ring-fired type and incorporating an inner water-wall type of furnace geometry increases the particle residence time. As a consequence, the burnout degree of the coal particles is constant without increasing the carbon content of the fly ash. However, these results can be ascribed to the over prediction of the furnace temperature as shown in Fig 5. Therefore, further research is needed for the validation of combustion models in terms of the coal devolatilization and char combustion models, and the radiative heat transfer model. In comparison to other performances, the temperature decrease in the furnace delays the ignition and burnout processes of the coal particles and also lowers the coal combustion rates for cases 3-5. Therefore, the temperatures at the furnace outlet for cases 3-5 are lower than those of cases 1 and 2 because of the cooling effect on the coal particles caused by both the outer and inner water walls. The Wall heat flux (WHF) values for cases 3-5 are more than 50% greater than those for cases 1 and 2. This is an indication of the heat absorption by the water-cooled walls, which decreases the mean temperature of the furnace outlet. The heat loss in terms of the flue gases is decreased owing to the decrease in the temperature at the furnace exit, and it is expected that the thermal efficiency of the boiler increases with an inner water wall. Furthermore, the decrease in temperature at the burner regions with an inner water wall reduces the formation of NO_x. Therefore, the NO_x concentrations at the furnace exit are significantly reduced for case 5, to as low as half of that for case 1.

The above results well match the particle behavior, as shown in Fig. 12, which shows the mean values of particle residence time and temperature for more than 1000000 particles under five different cases. The particle temperature and residence time have a complementary relationship. The parti-

Table 4. Summary of burnout, mean particle temperature, mean particle residence time, and heat flux under different boiler geometries.

		Case A	Case B	Case C	Case D	Case E
Burnout [%]		100	100	100	100	100
Mean particle temperature [K]		1787	1801	1739	1756	1749
Mean particle residence time [sec]		5.53	5.36	5.55	6.4	6.28
Heat flux [kW/m^2]	Outer wall	-	-	-96	-102	-104
	Inner wall	-	-	-108	-114	-115
	Total	-115	-137	-204	-216	-219

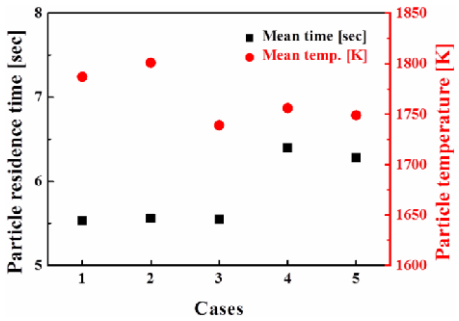

Fig. 12. Mean values for particle temperature and residence time under different furnace geometries.

cle residence time is 5.53 s for case 1, 5.36 s for case 2, 5.55 s for case 3, 6.4 s for case 4 and 6.28 s for case 5. The mean particle temperature is 1787 K for case 1, 1801 K for case 2, and approximately 1740 K for cases 3-5. The performance parameters are listed in Table 4. Models with an inner water wall were found to be better at reducing NO_x emissions without loss of the carbon burnout performance because of the increased particle residence time. There are two reasons for NO_x reduction by increasing the particle residence time and decreasing the particle temperature in the boiler. One is the cooling effect on the coal particles caused by both the outer and inner water walls. The particle temperature is lowered with increasing the particle residence time in the boiler because most of the coal particles are concentrated at the vicinity of both inner and outer water walls as shown in Fig. 4(c). The other is the air staged combustion. In the ring type boilers of this study, the OFA was applied based on case 1. The NO_x emission decreased with increasing the coal particle residence in the fuel rich zone (Burner zone) by numerous reported papers [6, 46-49].

In a comparison of cases 2-5 for ring fired type models, the mean temperature and NO_x emission in case 2 are relatively higher because the particle residence time is shorter than that of other cases. The velocity in the wind box zone, including the primary and secondary air, for case 2 is higher than that of other cases because of the reduced area of the burners. Moreover, the furnace length for case 2 is the shortest among the five models. On the basis of the above results, the inner water wall shows very positive effects on the particle residence time, temperature, and heat transfer, which can be expected to enhance the thermal efficiency of a furnace. Consequently, the NO_x emissions are reduced by 30% in comparison to models without an inner water wall. Further research focused on a more suitable combustion model for the validation, such as for coal devolatilization and char combustion, may be needed for considering these five cases, including various re- and superheaters. Unlike the tangentially fired boiler, even though the primary design concept of burner geometry for reducing NO_x emission in this study is to increase the particle residence time and to decrease the temperature in the boiler, the ring fired boiler is more likely to have the ash deposition problem at both inner and outer water walls. Therefore, the flexibility of the burner movement such as controlling yaw and tilt angles of the burner should be considered in the primary design concept of the burner geometry to alleviate the tube corrosion and heat balance problem at radiative water walls. Nevertheless, this study may provide useful information for controlling and reducing NO_x emissions by changing the geometric structures of the furnace.

4. Conclusions

The combustion performance and NO_x emissions of nontraditional ring-fired furnaces, including models with an additional inner water wall, based on a traditional 500 MW_e tangentially fired furnace, were numerically investigated using commercial CFD code. The main results can be summarized as follows:

(1) The ring-fired furnace was highly effective at utilizing the entire volume of the furnace in terms of enhancing the mixing of the oxidizer and coal particles. Moreover, coal particles were well distributed at the vicinity of the walls.

(2) The heat flux for models incorporating the inner water wall was approximately 50% higher than that of models without the inner water wall. The heat loss in terms of the flue gases was decreased by a decrease in temperature at the furnace exit, which increased the thermal efficiency of the boiler with an inner water wall.

(3) The adoption of an additional inner water wall had positive effects on the particle residence time, temperature, and heat transfer, which can be expected to enhance the thermal efficiency. Consequently, the NO_x emission was reduced by 30% in comparison to the models without an inner water wall.

(4) The particle temperature and residence time had a trade-off relationship. In particular, the adoption of an additional inner water wall provided a longer particle residence time in the burner zones for the reducing NO_x environment.

Acknowledgment

This work was supported by the Human Resources Development program *(No. 20144010200780)* of the Korea Institute of Energy Technology Evaluation and Planning (KETEP) grant funded by the Korea government Ministry of Trade, In-

dustry and Energy.

References

[1] Y. Sung, C. Moon, S. Ahn, G. Choi and D. Kim, Experimental study on interaction and excess heat release under oxy-fuel combustion of blended coals, *Korean J. Chem. Eng.,* 30 (2) (2013) 337-344.

[2] A. H. Al-Abbas, J. Naser and D. Dodds, CFD modelling of air-fired and oxy-fuel combustion in a large-scale furnace at Loy Yang a brown coal power station, *Fuel,* 102 (2012) 646-665.

[3] S. A. Skeen, B. M. Kumfer and R. L. Axelbaum, Nitric oxide emissions during coal/biomass combustion under air-fired and oxy-fuel conditions, *Energy Fuels,* 24 (2010) 4144-4152.

[4] T. D. B. Nguyen, Y. I. Lim, W. H. Eom, S. J. Kim and K. S. Yoo, Experiment and CFD simulation of hybrid SNCR-SCR using urea solution in a pilot-scale reactor, *Comput. Chem. Eng.,* 34 (2010) 1580-1589.

[5] L. D. Smoot, S. C. Hill and H. Xu, NO_x control through reburning, *Prog. Energy Combust. Sci.,* 24 (1998) 385-408.

[6] S. Munir, W. Nimmo and B. M. Gibbs, The effect of air staged, co-combustion of pulverised coal and biomass blends on NO_x emissions and combustion efficiency, *Fuel,* 90 (2011) 126-135.

[7] Q. Fang, A. A. B. Musa, Y. Wei, Z. Luo and H. Zhou, Numerical simulation of multifuel combustion in a 200 MW tangentially fired utility boiler, *Energy Fuels,* 26 (2012) 313-323.

[8] H. Tan, Y. Niu, X. Wang, T. Xu and S. Hui, Study of optimal pulverized coal concentration in a four-wall tangentially fired furnace, *Appl. Energy,* 88 (2011) 1164-1168.

[9] M. Y. Hwang, S. M. Kim, G. B. Kim, B. H. Lee, J. H. Song, M. S. Park and C. H. Jeon, Simulation studies on direct ash recycling and reburning technology in a tangentially fired 500 MW pulverized coal boiler, *Fuel,* 114 (2013) 78-87.

[10] W. Kim, D. J. Lee and S. W. Park, Experimental study on optimization of over-fire air in modified combustion with selective catalytic reduction, *J. Mech. Sci. Technol.,* 25 (4) (2011) 901-909.

[11] Y. G. Kim, B. H. Lee and C. H. Jeon, Combustion and emission characteristics of low rank-coals utilized in Korea, *J. Mech. Sci. Technol.,* 27 (9) (2013) 2857-2868.

[12] C. R. Choi and C. N. Kim, Numerical investigation on the flow, combustion and NO_x emission characteristics in a 500 MWe tangentially fired pulverized-coal boiler, *Fuel,* 88 (2009) 1720-1731.

[13] H. Liu, Y. Liu, G. Yi, L. Nie and D. Che, Effects of air staging conditions on the combustion and NO_x emission characteristics in a 600 MW wall fired utility boiler using lean coal, *Energy Fuels,* 27 (2013) 5831-5840.

[14] H. Liu, N. Xin, Q. Cao, L. Sha, D. Sun and S. Wu, Numerical simulation of the influence of over fire air position on the combustion in a single furnace boiler with dual circle firing, *Korean J. Chem. Eng.,* 26 (4) (2009) 1137-1143.

[15] L. Yan, B. He, F. Yao, R. Yang, X. Pei, C. Wang and J. Song, Numerical simulation of a 600 MW utility boiler with different tangential arrangements of burners, *Energy Fuels,* 26 (2012) 5491-5502.

[16] N. Modlinski, Computational modeling of a utility boiler tangentially-fired furnace retrofitted with swirl burners, *Fuel Process. Technol.* 91 (2010) 1601-1608.

[17] N. Spitz, R. Saveliev, M. Perelman, E. Korytni, B. Chudnovsky, A. Talanker and E. Bar-Ziv, Firing a sub-bituminous coal in pulverized coal boilers configured for bituminous coals, *Fuel,* 87 (2008) 1534-1542.

[18] I. Constenla, J. L. Ferrín and L. Saavedra, Numerical study of a 350 MWe tangentially fired pulverized coal furnace of the As Pontes power plant, *Fuel Process. Technol.,* 116 (2013) 189-200.

[19] *http://www.netl.doe.gov/File%20Library/Research/Coal/major%20demonstrations/cctdp/Round3/IntegDryNOxSO2/topical5.pdf.*

[20] *http://www.ee.co.za/wpcontent/uploads/legacy/En%20Sept%20GT%20Introducing2.pdf.*

[21] A. S. Fomichev and O. V. Pilipenko, Development and study of boilers with a ring furnace using different coals, *Power Technology and Engineering,* 44 (5) (2011) 400-405.

[22] R. V. Gubanov, V. A. Poloskov, V. P. Sennov and F. A. Serant, Twelve years' experience of successful adoption and operation of E-820 circular-furnace boiler, *Power Technology and Engineering,* 47 (1) (2013) 50-53.

[23] B. Kim, Boiler furnace that avoids thermal NO_x, *US Patent*, 0186828 (2007).

[24] M. J. Yoon, B. H. Lee, J. H. Song, G. B. Kim, Y. J. Chang and C. H. Jeon, Numerical study of the optimization of combustion and emission characteristics of air-staged combustion in a pulverized coal-fired boiler, *Trans. of the KSME (B),* 34 (6) (2010) 587-597.

[25] L. I. Díez, C. Cortés and J. Pallarés, Numerical investigation of NO_x emissions from a tangentially-fired boiler under conventional and overfire air operation, *Fuel,* 87 (2008) 1259-1269.

[26] S. V. Patankar, *Numerical heat transfer and fluid flow*, Hemisphere Publishing Corporation, New York, USA (1980).

[27] B. He, M. Chen, Q. Yu, S. Liu, L. Fan, S. Sun, J. Xu and W. Pan, Numerical study of the optimum counter-flow mode of air jets in a large utility furnace, *Comput. Fluids,* 33 (2004) 1201-1223.

[28] A. H. Al-Abbas, J. Naser and E. K. Hussein, Numerical simulation of brown coal combustion in a 550 MW tangentially-fired furnace under different operating conditions, *Fuel,* 107 (2013) 688-698.

[29] T. L. Bris, F. Cadavid, S. Caillat, S. Pietrzyk, J. Blondin and B. Baudoin, Coal combustion modelling of large power plant, for NOx abatement, *Fuel,* 86 (2007) 2213-2220.

[30] B. F. Magnussen and B. H. Hjertager, On mathematical modeling of turbulent combustion with special emphasis on soot formation and combustion, *Proc. Combust. Inst.,* 16

(1977) 719-729.
[31] Fluent Inc., *Fluent 6.3 User's Guide*, Lebanon, NH 03766, USA (2006).
[32] H. Knaus, R. Schneider, X. Han, J. Ströhle, U. Schnell and K. R. G. Hein, Comparison of different radiative heat transfer models and their applicability to coal-fired utility boiler simulations, *In: Fourth international conference on technologies and combustion for a clean environment*, Lisbon, Portugal (1997).
[33] R. V. Filkoski, Pulverised-coal combustion with staged air introduction: CFD analysis with different thermal radiation methods, *Open Thermodyn. J.,* 4 (4) (2010) 2-12.
[34] S. Park, J. A. Kim, C. Ryu, W. Yang, Y. J. Kim and S. Seo, Effects of gas and particle emissions on wall radiative heat flux in oxy-fuel combustion, *J. Mech. Sci. Technol.,* 26 (5) (2012) 1633-1641.
[35] L. Z. Zeng, Z. Li, G. Zhao, S. Shen and F. Zhang, Numerical simulation of combustion characteristics and NOx emissions in a 300 MWe utility boiler with different outer secondary-air vane angles, *Energy Fuels,* 24 (2010) 5349-5358.
[36] E. Karampinis, N. Nikolopoulos, A. Nikolopoulos, P. Grammelis and E. Kakaras, Numerical investigation Greek lignite/cardoon co-firing in a tangentially fired boiler, *Appl. Energy,* 97 (2012) 514-524.
[37] M. B. Gandhi, R. V. Vuthaluru, H. Vuthaluru, D. French and K. Shah, CFD based prediction of erosion rate in large scale wall-fired boiler, *Appl. Therm. Eng,.* 42 (2012) 90-100.
[38] M. Yang, Y. Y. Shen, H. T. Xu, M. Zhao, S. W. Shen and K. Huang, Numerical investigation of the nonlinear flow characteristics in an ultra-supercritical utility boiler furnace, *Appl Therm. Eng* (2014) http://dx.doi.org/10.1016/j.applthermaleng.2014.09.068.
[39] M. M. Baum and P. J. Street, Predicting the combustion behaviour of coal particles, *Combust. Sci. Technol.,* 3 (1971) 231-243.
[40] A. A. F. Peters and R. Weber, Mathematical modeling of a 2.4 MW swirling pulverized coal flame, *Combust. Sci. Technol.,* 122 (1997) 131-182.
[41] S. C. Hill and L. D. Smoot, Modeling of nitrogen oxides formation and destruction in combustion systems, *Prog. Energy Combust. Sci.,* 26 (2000) 417-458.
[42] C. Yin, S. Caillat, J. Harion, B. Baudoin and E. Perez, Investigation of the flow, combustion, heat-transfer and emissions from a 609 MW utility tangentially fired pulverized-coal boiler, *Fuel,* 81 (2002) 997-1006.
[43] L. D. Smoot, A decade of combustion research, *Prog. Energy Combust. Sci.,* 23 (1997) 203-232.
[44] B. R. Stanmore and S. P. Visona, Prediction of NO emissions from a number of coal-fired power station boilers, *Fuel Process. Technol.,* 64 (2000) 25-46.
[45] S. Xiu, Z. Li, B. Li, W. Yi and X. Bai, Devolatilization characteristics of biomass at flash heating rate, *Fuel,* 85 (2006) 664-670.
[46] W. Fan, Z. Lin, J. Kuang and Y. Li, Impact of air staging along furnace height on NOx emissions from pulverized coal combustion, *Fuel Process. Technol.,* 91 (2010) 625-634.
[47] A. Ribeirete and M. Costa, Impact of air staging on the performance of a pulverized coal fired furnace, *Proc. Combust. Inst.,* 32 (2009) 2667-2673.
[48] H. Spliethoff, U. Greul, H. Rüdiger and K. R. G. Hein, Basic effects on NOx emissions in air staging and reburning at a bench-scale test facility, *Fuel,* 75 (1996) 560-564.
[49] W. Bai, H. Li, L. Deng, H. Liu and D. Che, Air-staged combustion characteristics of pulverized coal under high temperature and strong reducing atmosphere conditions, *Energy Fuels,* 28 (2014) 1820-1828.

Yonmo Sung received his Ph.D. in Mechanical Engineering from Pusan National University in 2014. He is particularly interested in optical measurements of multi-phase reacting flows. Dr. Sung is currently an academic visitor at Imperial College London in UK.

Gyungmin Choi received his Ph.D. in Mechanical Engineering from Pusan National University in 1997 and from Osaka University in 2002. Dr. Choi is a professor in School of Mechanical Engineering, Pusan National University, Busan, Korea.